

Disulfidptosis-related lncRNAs Predict Prognosis and Immune Landscape in Endometrial Cancer

Yu Zhang¹, Yaping Wang^{1,2}, Xiabing Li¹, Qimin Jin¹, Hongjian Zhang¹, Hai Zhu¹, Qing Liu¹, Hongyu Li^{1,2,*}

¹Gynecologic Oncology, The Third Affiliated Hospital of Zhengzhou University, Zhengzhou, Henan, China.

²Zhengzhou Key Laboratory of Gynecological Oncology, Zhengzhou, Henan, China.

How to cite this paper: Yu Zhang, Yaping Wang, Xiabing Li, Qimin Jin, Hongjian Zhang, Hai Zhu, Qing Liu, Hongyu Li. (2024) Disulfidptosis-related lncRNAs Predict Prognosis and Immune Landscape in Endometrial Cancer. *International Journal of Clinical and Experimental Medicine Research*, 8(1), 165-179. DOI: 10.26855/ijcemr.2024.01.030

Received: January 17, 2024

Accepted: February 14, 2024

Published: March 12, 2024

***Corresponding author:** Hongyu Li, Gynecologic Oncology, The Third Affiliated Hospital of Zhengzhou University, Zhengzhou, Henan, China; Zhengzhou Key Laboratory of Gynecological Oncology, Zhengzhou, Henan, China.

Abstract

Background: Recently, a novel form of cell death called disulfidptosis was identified. It is characterized by rapid cell death caused by disulfide stress resulting from excessive cystine accumulation within cells. Disulfidptosis holds promise as a potential target for intervention in tumor treatment. However, the roles and prognostic value of disulfidptosis-related lncRNAs (DRLs) in EC remain largely unknown. Therefore, the objective of this study is to develop a prediction model based on DRLs to forecast the prognosis and assess the immunotherapy response in EC patients, as well as identify potential chemotherapy drugs for treatment. **Methods:** We constructed a model by screening DRLs associated with EC prognosis through bioinformatics methods and validated it. Furthermore, enrichment analysis was conducted to explore functional differences between different risk populations. Additionally, we examined the associations between the risk score and tumor mutational burden (TMB), tumor microenvironment (TME), tumor immune dysfunction and exclusion (TIDE), and drug sensitivity. Finally, we validated this using quantitative reverse transcription polymerase chain reaction (qRT-PCR). **Results:** We identified 8 DRLs (Z69733.1, AL158071.4, AC022960.1, AC005034.2, AC003086.1, AC024230.1, AL499602.1, RAB11B-AS1) and constructed a robust risk model. Further analysis revealed that the low-risk group had superior overall survival (OS), immunotherapy response, and drug sensitivity compared to the high-risk group. **Conclusion:** Our risk model provides an accurate prediction of prognosis and immunotherapy response in EC patients, offering significant clinical implications and novel insights for clinicians in the treatment of EC.

Keywords

Endometrial cancer, Disulfidptosis, Long noncoding RNA, Prognosis, Immune

1. Introduction

According to the Global Cancer Statistics of 2020, the incidence of endometrial cancer (EC) reached 417,000 new cases worldwide this year, accounting for 4.5% of all cancers and ranking second among female reproductive system tumors, surpassed only by cervical cancer. Surprisingly, despite its lower incidence rate, EC has the third highest mortality rate [1]. Currently, the primary approach for EC treatment involves surgery, complemented by radiotherapy and chemotherapy. Surgery remains the gold standard, while adjuvant therapies are determined based on various risk factors and pathological findings, such as age, histological grade, tumor size, depth of invasion, and lymph node status [2]. Recent advancements in immunotherapy and targeted therapy have shown promise in EC treatment [3]. Nonetheless, the prognosis for advanced and recurrent EC remains unfavorable. Therefore, the identification of new

therapeutic targets and biomarkers for EC is of utmost importance.

Regulatory cell death (RCD) plays a pivotal role in tumor treatment, encompassing various modes such as apoptosis, pyroptosis, autophagy, ferroptosis, and cuproptosis [4-6]. Recently, Liu *et al.* identified a novel form of cell death known as disulfidptosis, characterized by rapid demise due to disulfide stress resulting from intracellular cystine accumulation. The excessive buildup of disulfide disrupts the actions of disulfide bonds, activating a cascade of agonistic events and ultimately leading to cell death. In this study, cancer cells with aberrant expression of SLC7A11 exhibited heightened cystine uptake during glucose starvation. Reduction of cystine to cysteine resulted in the depletion of nicotinamide adenine dinucleotide phosphate (NADPH), leading to the massive accumulation of intracellular disulfides and subsequent cell death. Therapeutic strategies targeting disulfidptosis in tumor therapy have been proposed [7]. Previous work by Liu *et al.* demonstrated the crucial role of SLC7A11 in maintaining intracellular glutathione levels and protecting cells from oxidative stress-induced cell death, such as ferroptosis. SLC7A11 is frequently overexpressed in tumors, and their findings elucidated that cell death induced under glucose starvation conditions is distinct from cytoptosis and ferroptosis, providing the foundation for the subsequent discovery of disulfidptosis [8]. Zhang *et al.* further elucidated the specific mechanisms underlying disulfidptosis, opening up new avenues for targeted tumor therapy [9]. Additionally, Zhong *et al.* identified the involvement of nuclear factor of activated T cells 1 (NFATc1)-mediated upregulation of SLC7A11 in conferring metabolic sensitivity to TXNRD1 inhibitors during osteoclast differentiation, proposing that TXNRD1 inhibitors selectively eliminate osteoclast precursors by inducing intracellular cystine accumulation and subsequent disulfidptosis [10]. These studies collectively demonstrate the links between disulfidptosis and tumors, highlighting its potential as a target for tumor treatment. Disulfidptosis holds promise as a novel therapeutic approach for tumors that are resistant to apoptosis and unresponsive to conventional treatments. Thus, investigating the role of disulfidptosis in tumors has substantial clinical implications.

Long noncoding RNAs (lncRNAs) are a class of RNA molecules characterized by their length exceeding 200 base pairs and their lack of an open reading frame, rendering them devoid of coding protein function [11-13]. Numerous studies have highlighted the regulatory role of lncRNAs in various biological processes of tumors, underscoring their significance in tumorigenesis and tumor progression [14-17]. For instance, Ren *et al.* identified LUCAT1 as highly expressed in non-small cell lung cancer tissues, with its expression levels correlating with tumor size, TNM stage, lymphatic metastasis, overall survival (OS), and tumor proliferation capacity, which was attenuated upon knockdown [18]. Additionally, LUCAT1 has been investigated in other malignancies, such as cervical cancer [18], renal cancer [18], breast cancer [18], ovarian cancer [18], and prostate cancer [18], where its expression levels are upregulated. In the context of bladder cancer, Cao *et al.* observed elevated expression of lncRNA-RMRP in tumor tissues, which was closely associated with tumor size, lymph node status, and patient survival time. Suppression of lncRNA-RMRP expression led to diminished tumor proliferation, invasion, and migration capabilities [19]. Although numerous studies have explored differentially expressed lncRNAs in EC compared to normal tissues, the role of disulfidptosis-related lncRNAs (DRLs) in EC remains largely unknown.

The objective of this study was to construct a model of DRLs using bioinformatics approaches to assess prognosis and immunological features and identify potential therapeutic drugs for EC patients.

2. Materials and methods

2.1 Data acquisition

Uterine corpus endometrial carcinoma (UCEC) mRNA expression profiles and clinical data were downloaded from the TCGA database (<https://portal.gdc.cancer.gov>). The Perl programming language and R were used to process the data and extract the expression profiles of coding genes and lncRNAs, as well as the clinical information of EC patients, including age, stage, histological grade, survival status, and survival time.

2.2 Differential Expression Analysis of DRLs

A total of 10 disulfidptosis-related genes, including GYS1, NDUFS1, OXSM, LRPPRC, NDUFA11, NUBPL, NCKAP1, RPN1, SLC3A2, and SLC7A11, were obtained from published articles [7]. Screening for disulfidptosis-associated lncRNAs was performed using the Pearson correlation coefficient method with the "limma" package, with the screening condition set as $|\text{CorFilter}| > 0.4$, $p < 0.001$.

2.3 Construction and verification of the risk model

The cohort of EC patients was randomly divided into two sets: a testing set ($n=272$) and a training set ($n=272$).

Univariate Cox regression analysis and least absolute shrinkage and selection operator (LASSO) regression analysis were employed to screen for prognosis-related DRLs. Subsequently, multivariate Cox regression analysis was conducted to select independent prognostic markers in EC patients. The accuracy of the selected markers was assessed using the testing set and training set. The risk score was calculated using the following formula: Risk score = $\sum \text{coef}(\text{lncRNA}) \times \text{Exp}(\text{lncRNA})$, where $\text{coef}(\text{lncRNA})$ represents the regression coefficient and $\text{Exp}(\text{lncRNA})$ represents the expression of lncRNAs. Furthermore, the entire TCGA-UCEC set was divided into a high-risk set and a low-risk set based on the median risk score. Kaplan–Meier (KM) survival analysis was performed to compare differences in overall survival (OS) among the entire set, training set, and testing set.

2.4 Independent prognostic analysis and nomogram construction

To compare the advantages and limitations of the risk score with other clinical information, univariate and multivariate Cox regression analyses were performed to evaluate age, clinical stage, histological grade, and the risk score. The results were visualized using the "survival" package to determine whether the risk score served as an independent prognostic factor for EC patients. Additionally, the "survminer" and "timeROC" packages were employed to visualize the receiver operating characteristic (ROC) curves and the area under the curves (AUCs) of 1-, 3-, and 5-year survival. This evaluation aimed to assess the predictive performance and compare it with age, histological grade, and clinical stage. The C-index was used to assess the predictive effect. Based on the results of univariate and multivariate Cox regression analyses, the "rms" and "regplot" packages were utilized to construct a nomogram model for predicting the overall survival (OS) of EC patients at 1, 3, and 5 years. Additionally, calibration curves were employed to assess the reliability of the constructed nomogram model.

2.5 Principal component analysis (PCA) and functional enrichment analysis

PCA, as a widely employed algorithm for reducing data dimensionality, was utilized to demonstrate the distribution of gene expression profiles of EC patients across different hierarchical classifications. The resulting scatter plots were visualized using the "scatterplot3d" package. To analyze the differences in biological function between the high-risk and low-risk sets, the "limma" package was employed. Functional enrichment analysis, including Gene Ontology (GO) enrichment analysis, Kyoto Encyclopedia of Genes and Genomes (KEGG) enrichment analysis, and Gene Set Enrichment Analysis (GSEA), was performed. The "clusterProfiler", "enrichplot", and "org.Hs.e.g.db" packages were used to conduct the enrichment analysis and interpret the results.

2.6 Analysis of tumor mutational burden (TMB)

Mutation data of UCEC were downloaded from the TCGA database (<https://portal.gdc.cancer.gov>). EC patients were divided into sets based on their tumor TMB scores, using the median TMB score as the threshold. The 15 genes with the highest mutation frequency were visualized as waterfall plots using the "maftools" package in R. Next, the TMB score was integrated with the clinical information of EC patients. Survival analysis was conducted using the KM method to investigate the correlation between the TMB score and clinical data.

2.7 Tumor microenvironment (TME) analysis and tumor immune dysfunction and exclusion (TIDE) analysis

The estimate algorithm in the "estimate" package of R language was used to estimate the ratio of ImmuneScore, StromalScore, and ESTIMATEScore (ImmuneScore + StromalScore) of each sample in TME, and the "ggpubr" package visualized the results. Meanwhile, to evaluate immune cell infiltration and associated immune functions in EC patients, the infiltration rates of different types of immune cells in tumor samples were evaluated using the CIBERSORT algorithm. The "GSVA" and "GSEABase" packages were used to calculate the activities of immune-related pathways in different risk populations. We escaped from a tumor TIDE website (<http://tide.dfci.harvard.edu/>) to download the data using the "limma" and "ggpubr" packages for data processing and visualization.

2.8 Drug screening

The R packages "pRRophetic", "ggplot" and "ggpubr" were used to screen potential therapeutic drugs and observe drug sensitivity, and the screening condition was set to $p\text{Filter}=0.001$.

2.9 Cell culture and quantitative real-time PCR (qRT-PCR)

The human normal endometrial cell line icell-0031a (primary Yamaguchi cell base medium containing 2% fetal

bovine serum, iCell Bioscience Inc, Shanghai) and EC cell lines Ishikawa (1640 medium containing 10% fetal bovine serum,) and HEC-1-A (1640 medium containing 10% fetal bovine serum, BI, USA) were cultured in an incubator containing 5% carbon dioxide at a temperature of 37°C. Total cellular RNA was extracted using TRIzol (TransGen Biotech, China) and then reverse transcribed using Prime Script RT Master Mix (TOYOBO, Japan) to synthesize cDNA. RAB11B-AS1 was quantified by qRT-PCR using SYBR Green qPCR Master Mix (CW BIO, China) and specific primers. The specific primer sequences are as follows: The sequences of primers were as follows: for GAPDH, 5'-GGAGTCCACTGGCGTCTTCA-3'(forward), 5'-TCATGAGTCCTCCACGATACC-3'(forward); for RAB11B-AS1, 5'-GCGAAGCCAATCAGAGATGG-3' (forward), 5'-CTTGAGCTCGCCCTGATAG-3' (reverse) [20].

2.10 Statistical analysis

Perl (V5.32.1) extracted and integrated the data, and R (V4.2.2) analyzed the data and visualized the results. We used chi-square tests to compare subgroup clinical information parameters. The Pearson correlation test was suitable for correlation analysis. Comparisons between groups were made using the Kruskal–Wallis test. All analyses were two-sided, and $p < 0.05$ was considered statistically significant.

3. Results

3.1 Risk model based on DRLs

The flow chart of the study is shown in Fig. 1. By comparing the mRNA sequencing data and clinical information of UCEC patients (including 23 normal samples and 554 EC samples) in TCGA, we obtained 469 DRLs using the Perl and R language "limma" package. The co-expression relationship between DRLs and genes related to disulfidptosis was visualized using a mulberry diagram (Fig. 2A). Subsequently, 49 DRLs were obtained through univariate Cox regression analysis and LASSO regression analysis (Figs. 2B, C), with 45 considered risk factors and the remaining 4 as protective indicators (Fig. 2D). Furthermore, 8 candidate DRLs associated with OS were identified through multivariate Cox analysis. A risk model was built using a total of 8 DRLs: Z69733.1, AL158071.4, AC022960.1, AC005034.2, AC003086.1, AC024230.1, AL499602.1, and RAB11B-AS1. The correlation heatmap displayed the relationship between genes related to disulfidptosis and the 8 DRLs (Fig. 2E).

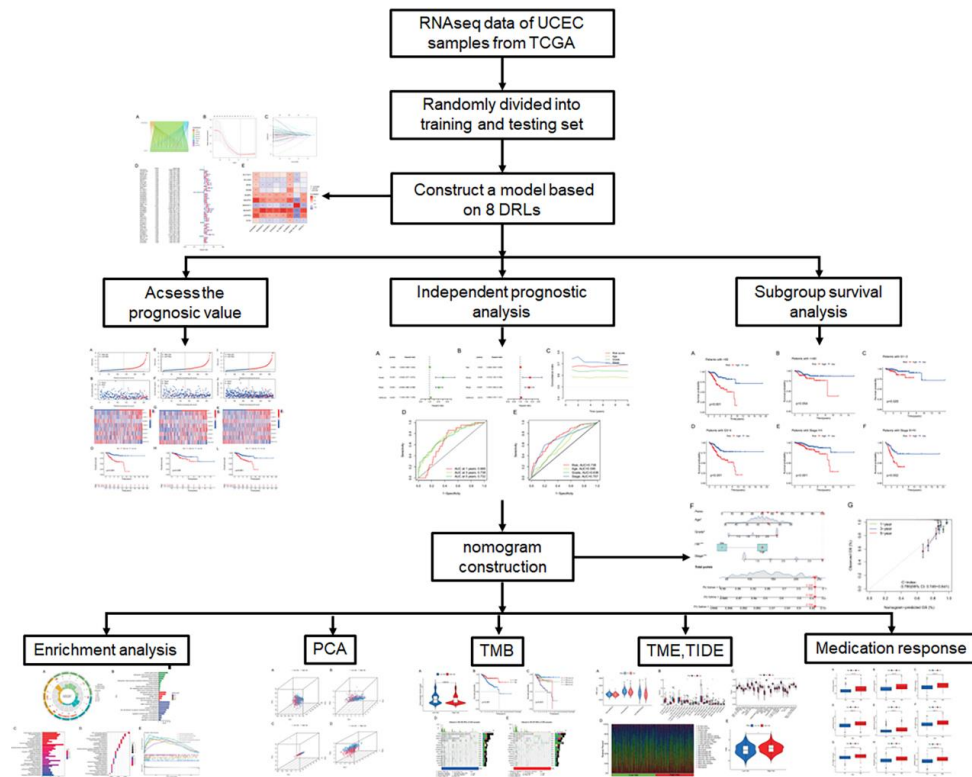


Figure 1. Flow chart of this study.

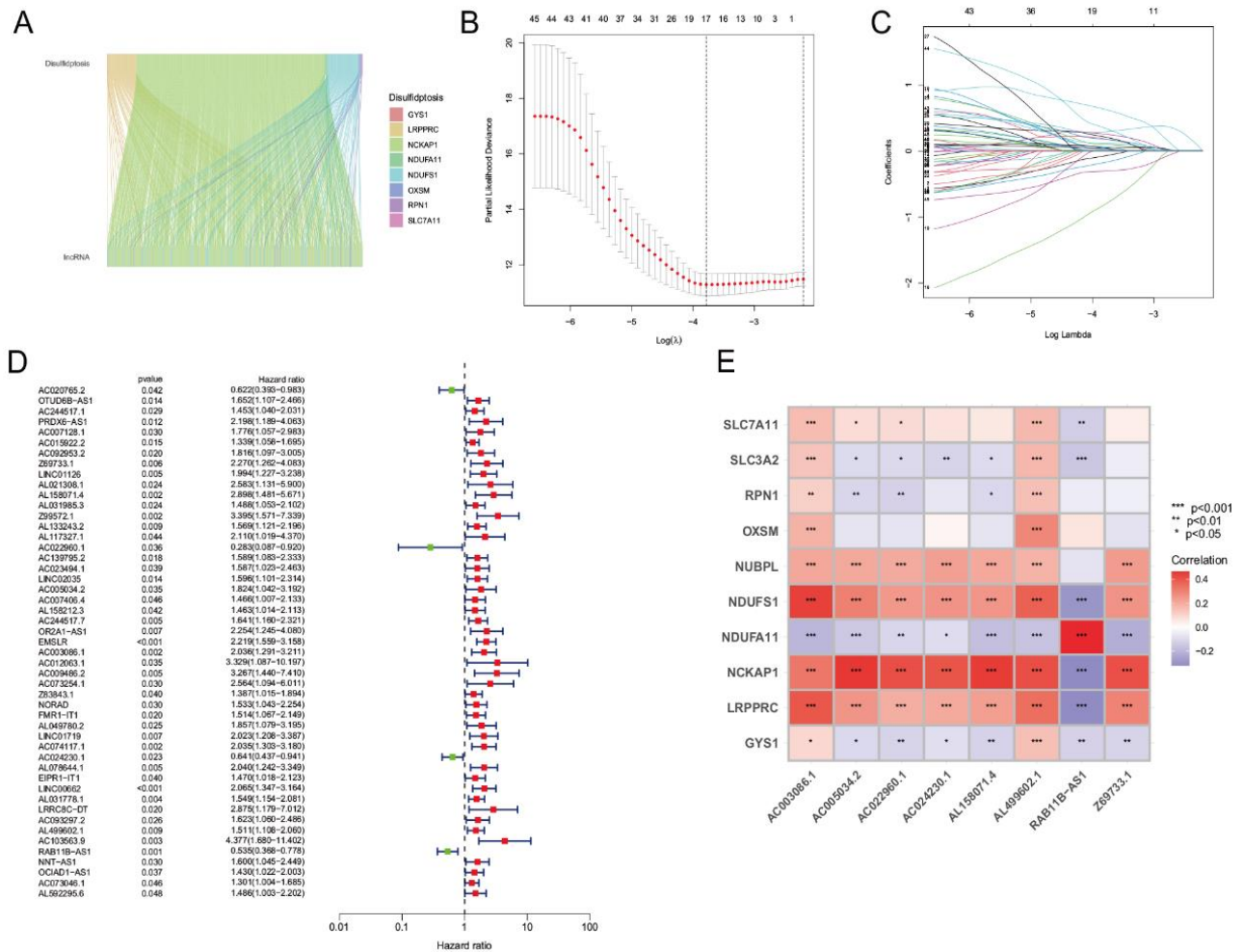


Figure 2. Identification of the signature of disulfidptosis-related lncRNAs.

A: The mulberry map shows the relationship between disulfidptosis-related genes and lncRNAs.

B: Cross-validation curve for LASSO regression analysis.

C: LASSO coefficient of DRLs.

D: Forest map showing DRLs that were screened by univariate Cox regression analysis and correlated with prognosis.

E: The heatmap shows the relationship between DRLs and genes in the risk model.

3.2 The risk score was used to predict the prognosis of EC patients

EC patients were divided into a high-risk set and a low-risk set for survival analysis using the median risk score. The risk was calculated using the following equation: Risk score = $Z69733.1 \times 0.623675510005963 + AL158071.41.15167191478137 + AC022960.1 \times (-1.56340059988008) + AC005034.2 \times 0.590688044797002 + AC003086.1 \times 0.494338175388747 + AC024230.1 \times (-0.331597815468645) + AL499602.1 \times 0.337198223520806 + RAB11B-AS1 \times (-0.548639480466623)$. The results indicated that patients in the low-risk set had significantly better OS than those in the high-risk set. Moreover, an increase in the risk score was associated with higher mortality in EC patients (Figs. 3A, B, D). Similar trends were observed in the testing and training sets (Figs. 3E, F, H, I, J, L). In the entire set, training set, and testing set, the expression levels of Z69733.1, AL158071.4, AC005034.2, AC003086.1, and AL499602.1 were higher in the high-risk set, suggesting that these DRLs are potential poor prognostic factors. Conversely, the expression levels of AC022960.1, AC024230.1, and RAB11B-AS1 were lower in the high-risk set, indicating that these DRLs are potential protective factors (Figs. 3C, G, K). Additionally, the OS and clinical characteristics of EC patients were compared based on age, clinical stage, and histological grade. The results showed that, except for patients under the age of 60 (Figs. 4A, B), the OS of high-risk patients was shorter than that of low-risk patients (Figs. 4C, D, E, F).

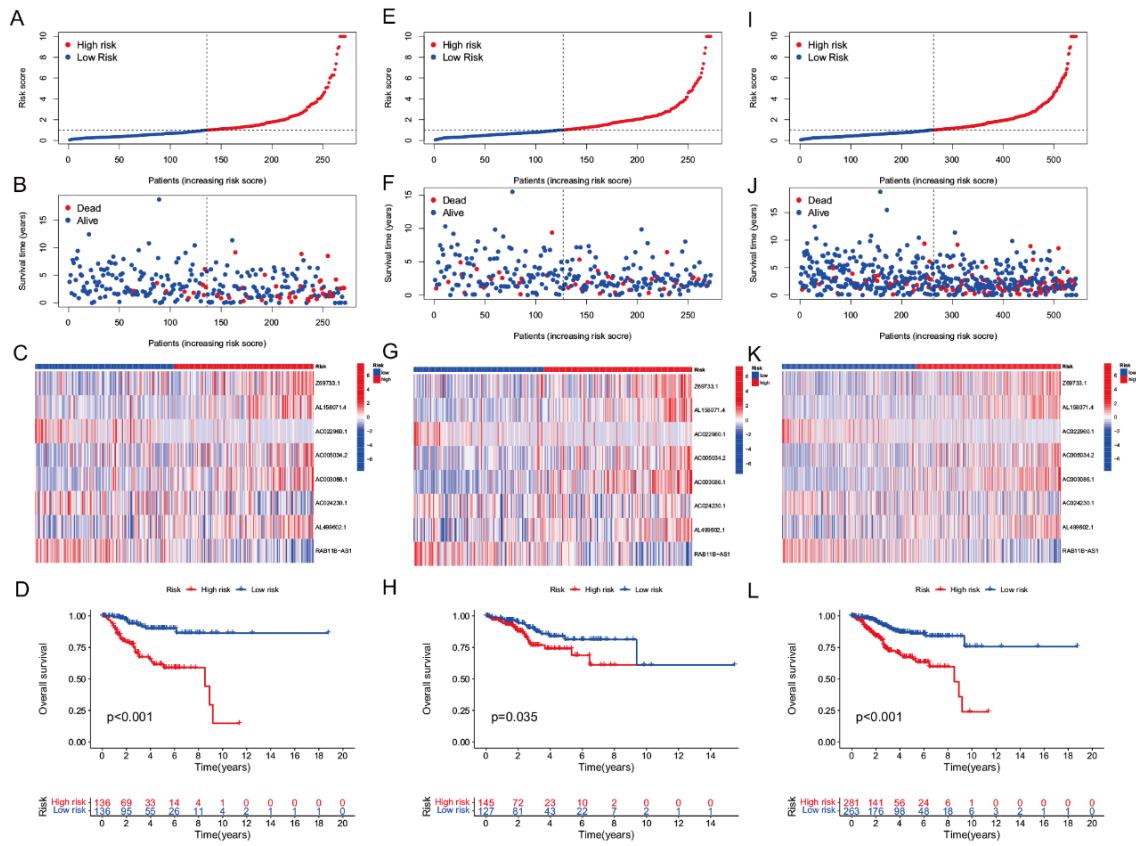


Figure 3. Effect of DRLs on prognosis. (A-D) Training set. (E-H) Testing set. (I-L) Entire set. (D, H, L) KM survival analysis of OS in low- and high-risk sets. (A, B, C) The distribution of the risk scores for categorized patients. (D, E, F) The distribution of classified patient survival status with increasing risk score. Blue represents the survivors, and red represents the dead. (G, H, I) Expression of DRLs in different risk populations.

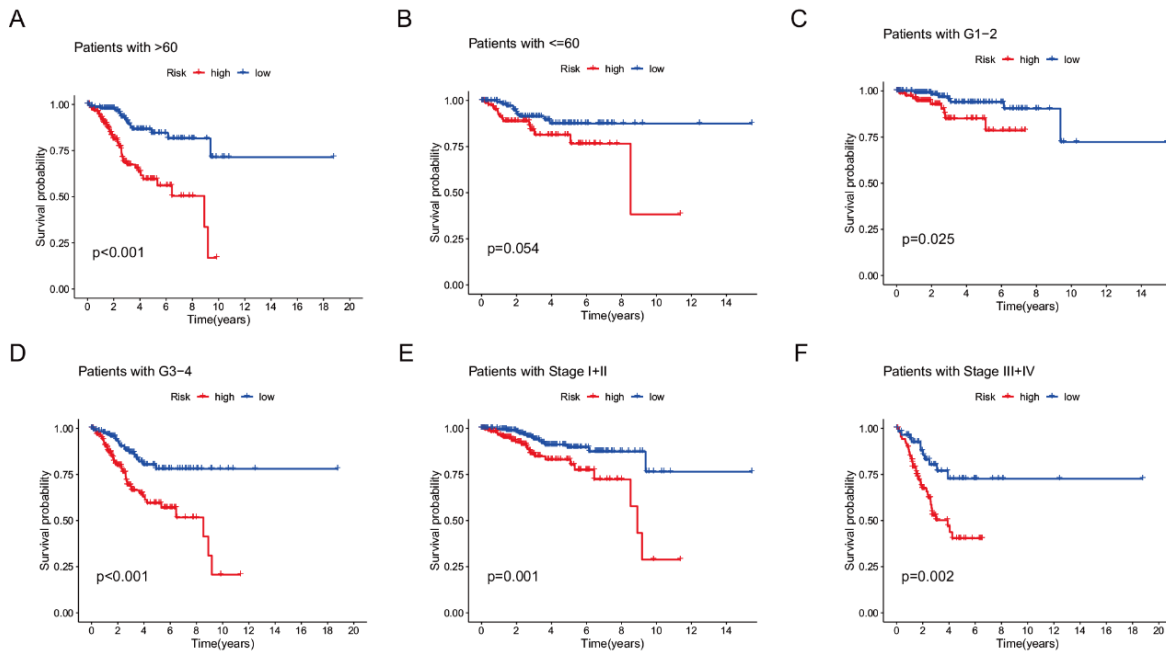


Figure 4. KM survival analysis of different subgroups in low- and high-risk sets. (A, B) Age. (C, D) Histological grade. (E, F) Clinical stage.

3.3 Independent prognostic analysis and nomogram construction

Based on univariate and multivariate Cox regression, the risk score was confirmed as an independent prognostic factor in EC patients (Figs. 5A, B). The AUCs for 1, 3, and 5 years were 0.666, 0.738, and 0.732, respectively (Figs. 5D). The AUC of the risk score was 0.738, indicating better predictive power than other clinical features (Fig. 5E). Furthermore, we found that the C-index of the risk score had higher scores than other clinical variables at the 10-year mark, suggesting that the risk score may be a reliable prognostic indicator to predict long-term clinical outcomes in EC patients (Fig. 5C). Moreover, a nomogram was constructed using age, histological grade, risk score, and clinical stage to predict the 1-, 3-, and 5-year survival probabilities of EC patients. The total score for a selected patient was 241, resulting in 1-, 3-, and 5-year OS probabilities of 0.799, 0.346, and 0.226, respectively (Fig. 5F). Calibration curves confirmed the predictive power of the prognostic model, showing a strong agreement between clinical nodal status and predicted survival (Fig. 5G). These results suggested that the risk score may be a potent prognostic indicator for predicting clinical outcomes in EC patients.

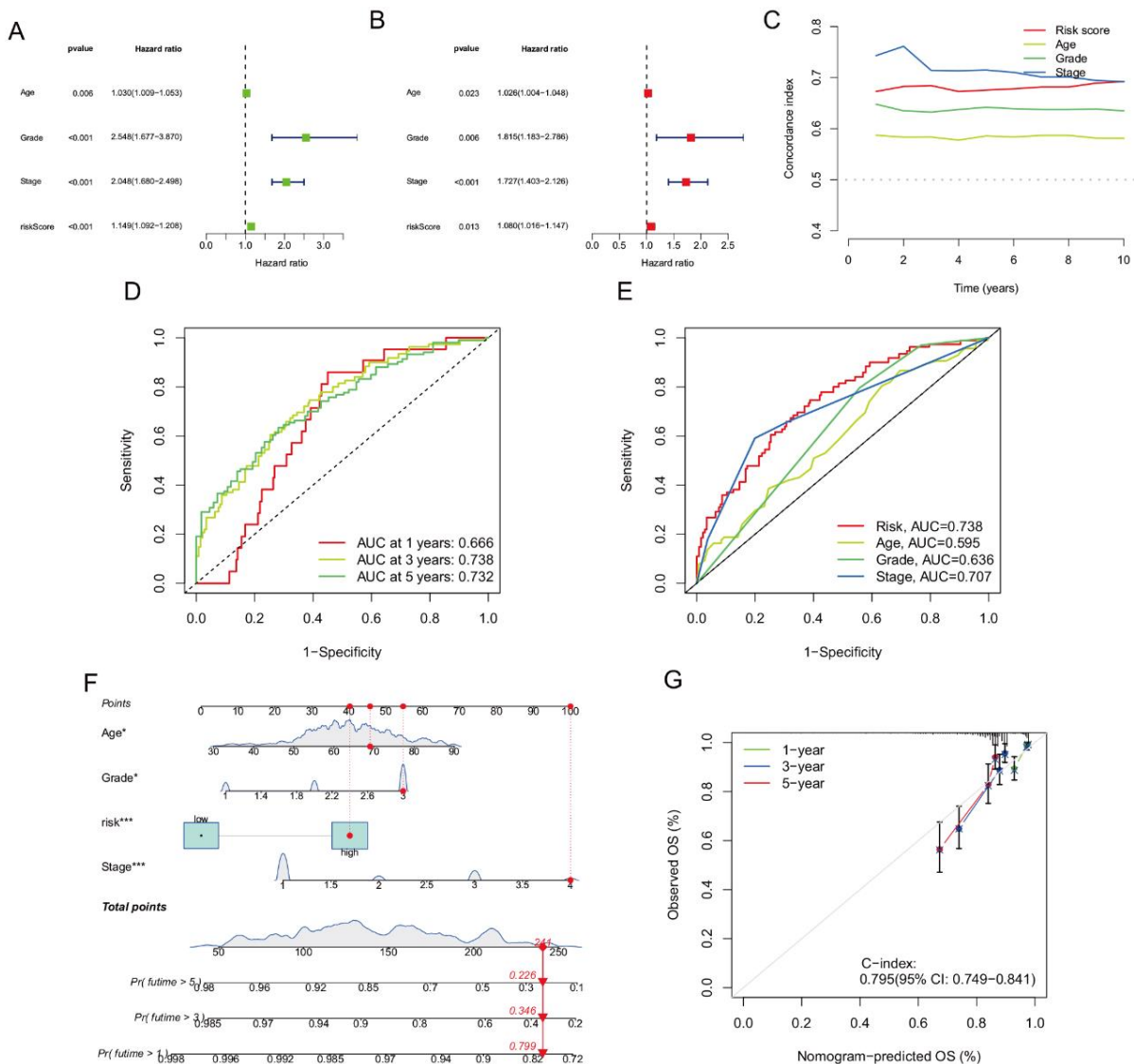


Figure 5. Verification of the constructed lncRNA model related to disulfidptosis and construction of a column graph with predictive value. **A:** Univariate Cox regression analysis of clinical characteristics and risk score. **B:** Multivariate Cox regression analysis of clinical characteristics and risk score. **C:** The C index of clinical characteristics and risk score. **D:** Time-dependent ROC curves of the risk model. **E:** Comparison of AUCs among the risk model and clinical characteristics. **F:** A nomogram combining clinical information and risk score that predicted the 1-, 3-, and 5-year survival rates of patients. **G:** Calibration curves that reflected the accuracy of the nomogram.

3.4 PCA and functional enrichment analysis (GO analysis, KEGG analysis, GSEA)

PCA was performed to assess the distribution patterns, as depicted in Fig. 6. The three-position scatter plot of PCA revealed the distribution of EC patients according to different classification models, including DRLs, disulfidptosis-related genes, and all genes. The results demonstrated that the model constructed using lncRNAs achieved superior classification of EC patients into high-risk and low-risk sets compared to other models. Subsequent functional enrichment analysis uncovered significant enrichment in several biological processes (BP), such as axon development, pattern specification process, and axonogenesis. Additionally, in the field of cell components (CC), enrichment was observed in the endoplasmic reticulum lumen, immunoglobulin complex, and collagen trimer. Regarding molecular function (MF), receptor ligand activity and extracellular matrix structural constituent were the enriched terms (Figs. 7A, B). Furthermore, KEGG analysis revealed enrichment in pathways including the PI3K-Akt signaling pathway and Wnt signaling pathway, among others (Figs. 7C, D). GSEA demonstrated enrichment of pathways such as the calcium signaling pathway, cell adhesion molecules cams, ECM receptor interaction, neuroactive ligand-receptor interaction, and pathways in cancer within the high-risk group (Fig. 7E). Overall, these findings suggest a potential relationship between these DRLs and immunity.

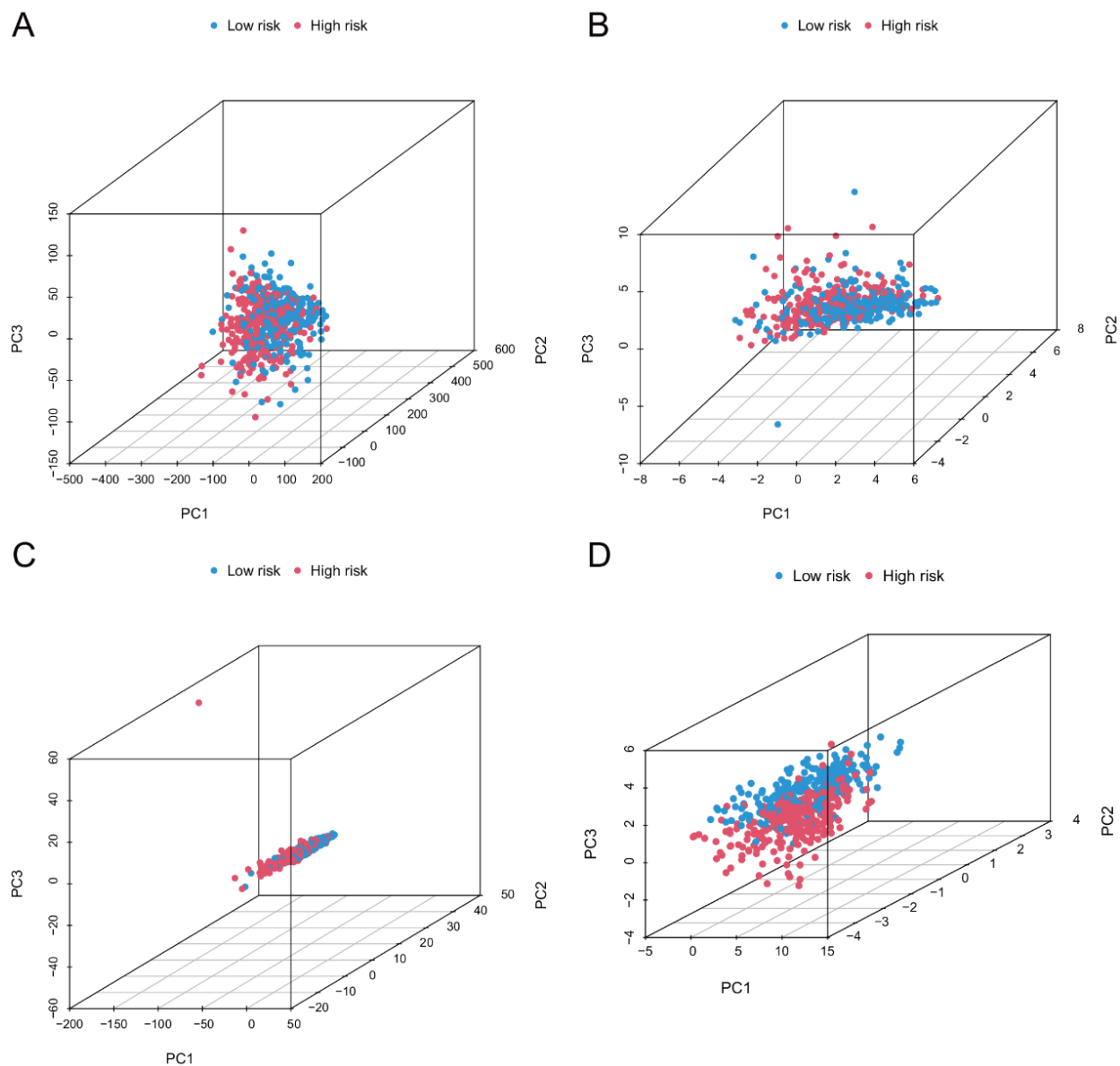


Figure 6. Principal component analysis. A: All genes. B: Disulfidptosis-related gene. C: DRLs. D: Risk model constructed by DRLs.

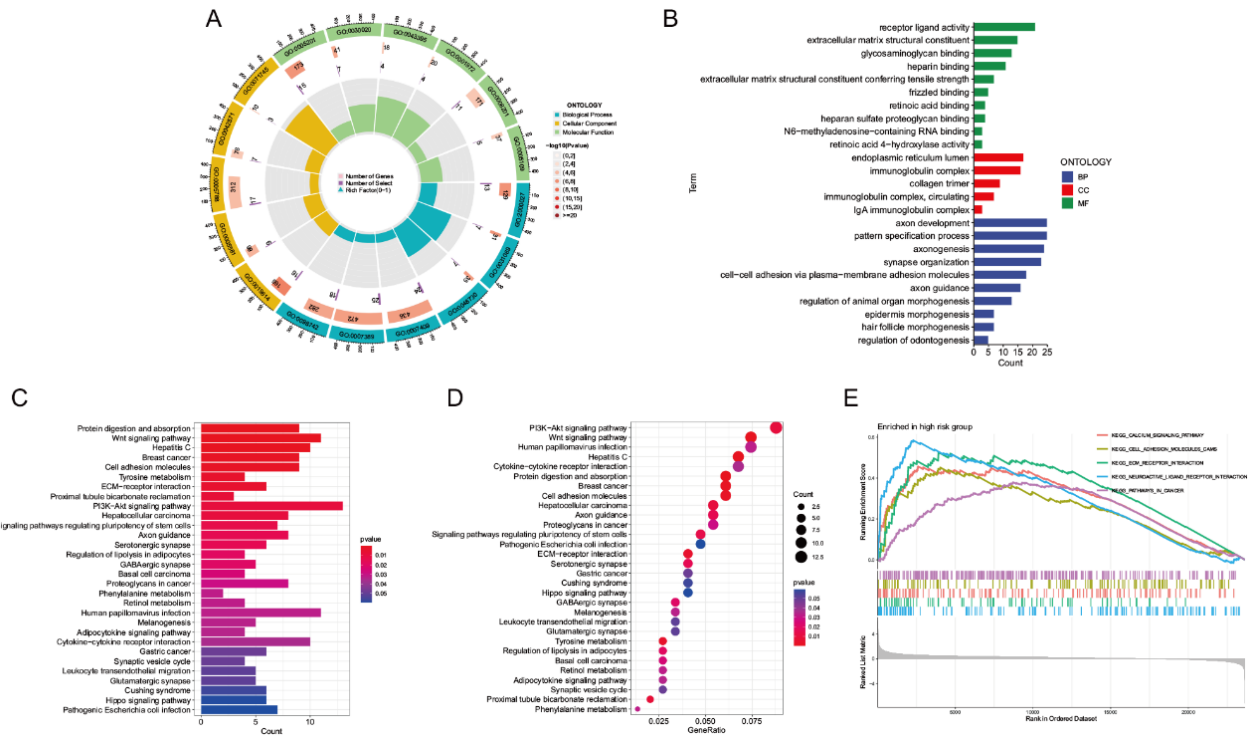


Figure 7. Biological function enrichment analysis. A: Circle plots for the GO analysis. B: GO analysis of DEGs between high- and low-risk sets. (C, D) KEGG analysis of DEGs between high- and low-risk sets. E: GSEA demonstrating the top five enriched pathways in high-risk sets.

3.5 Analysis of TMB

To analyze the changes in somatic mutations between the high- and low-risk sets, we obtained somatic mutation data from The Cancer Genome Atlas (TCGA) database (<https://portal.gdc.cancer.gov>). The top 15 genes with the highest mutation rates included PTEN, PIK3CA, ARID1A, TTN, TP53, PIK3R1, KMT2D, CTNNB1, MUC16, CTCF, CSMD3, ZFH3, KMT2B, RYR2, and DST. The results indicated that the gene mutation frequency was generally lower overall in the high-risk set than in the low-risk set. However, significantly more common mutations were observed in TP53 within the high-risk set (Figs. 8D, E). A comparison was made between the frequency of tumor gene mutations and the difference in TMB across the different risk sets. The results revealed a significant difference in TMB between the low-risk set and the high-risk set ($p < 0.001$, Fig. 8A), with the high TMB group exhibiting a better prognosis than the low TMB group (Fig. 8B). Furthermore, by combining TMB with the risk score, the entire cohort was classified into four distinct groups (H-TMB + high risk, H-TMB + low risk, L-TMB + high risk, and L-TMB + low risk). A comparison of OS among the four groups demonstrated that the H-TMB + high-risk group had the best prognosis, while the L-TMB + high-risk group had the worst prognosis ($p < 0.001$, Fig. 8C).

3.6 TME analysis and TIDE analysis

Considering the pivotal role of the TME and the transformative impact of immune checkpoint inhibitors in tumors, we conducted an analysis of the TME in the high- and low-risk sets. The results revealed notable disparities in ImmuneScore, StromalScore, and ESTIMATEScore between the two sets, with significant differences observed in the latter two scores ($p < 0.001$). Specifically, the low-risk set exhibited higher scores than the high-risk set (Fig. 9A). Differential analysis of immune cell infiltration indicated an upregulation of B cell naive and activated dendritic cells in the high-risk set. In contrast, Tregs showed downregulation in the high-risk set ($p < 0.05$, Figs. 9B, D). Additionally, we explored the relationship between the risk score and immune function in EC. The box plot (Fig. 9C) illustrated marked differences in APC costimulation, checkpoint expression, cytolytic activity, human leukocyte antigen (HLA) presentation, and inflammation-promoting factors, indicating heightened immune activity in the low-risk set. TIDE is a recently developed method for predicting the efficacy of immune checkpoint inhibitors [21], as

well as estimating OS. To further investigate immune escape mechanisms in different risk sets, we obtained tumor immune escape scores from the TIDE website (<http://tide.dfci.harvard.edu/>). The results demonstrated significantly lower tumor immune escape scores in the low-risk set than in the high-risk set ($p < 0.01$, Fig. 9E), implying more pronounced immune escape in the high-risk set and poor response to immunotherapy.

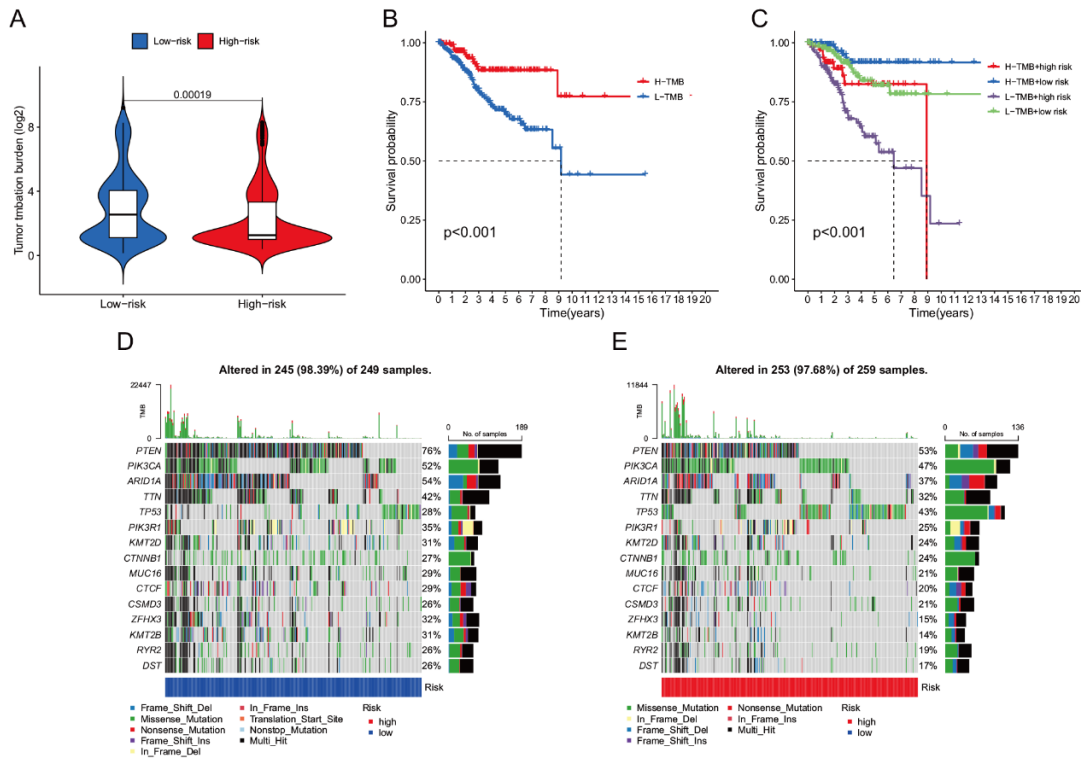


Figure 8. Relationship between TMB and the constructed model. A: Violin plot of TMB between high- and low-risk sets. **B:** KM survival analysis between high- and low-TMB sets. **C:** KM survival analysis of TMB combined risk scores. **D:** Waterfall map of the top 15 genes with high mutation frequency in the low-risk set. **E:** Waterfall map of the top 15 genes with high mutation frequency in the high-risk set.

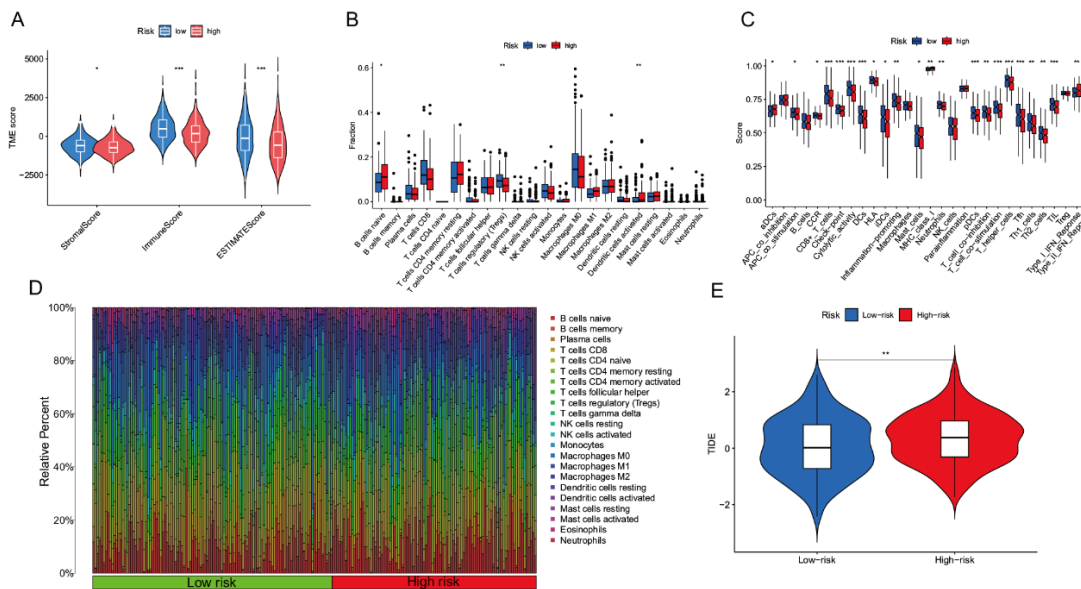


Figure 9. TME analysis and TIDE analysis between high- and low-risk sets. A: Comparison of Immune Scores, StromalScores, and ESTIMATEScores between the high- and low-risk sets. **B, D:** Differences in immune cell infiltration between high- and low-risk sets. **C:** Differences in immune function between high- and low-risk groups. **E:** TIDE analysis between high- and low-risk groups.

3.7 Drug susceptibility analysis

To identify potentially effective antineoplastic drugs, we employed the "pRRophetic" package to analyze the differential sensitivities to drugs between the two sets, where lower IC₅₀ values indicate greater drug sensitivity. Subsequently, we identified nine drugs that exhibited significant differences in susceptibility between the two sets. These drugs included AZD6482, Afuresertib, Mitoxantrone, PRT062607, AZD2014, Dabrafenib, PF-4708671, AZD8055, and MK-2206. Notably, the low-risk set of patients displayed higher sensitivity to these drugs compared to the high-risk set (Figs. 10A-I). These findings hold considerable promise and serve as a valuable reference for clinical medication decisions in patients with EC.

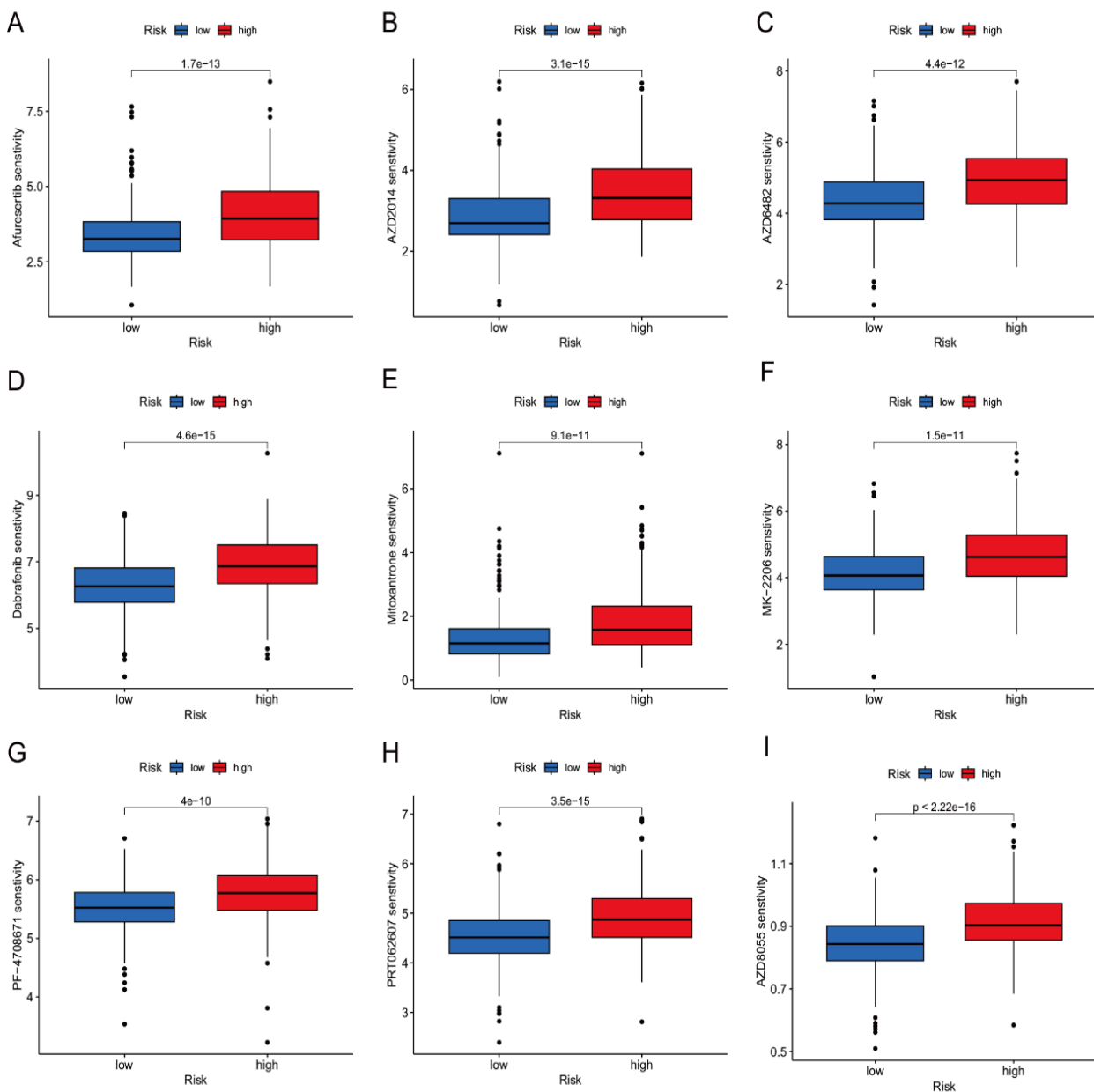
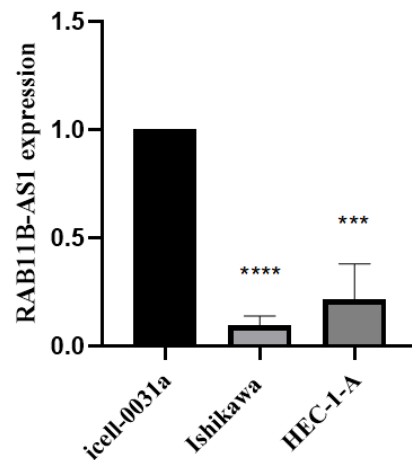


Figure 10. Drug sensitivity analysis. (A-I) Potential 9 drugs for EC.

3.8 Validation of RAB11B-AS1 expression

Consistent with our expectation, the expression of RAB11B-AS1 was down-regulated in EC cell lines Ishikawa and HEC-1-A compared with normal endometrial cells (Fig. 11).



The expression of RAB11B-AS1 in 3 cell lines

Figure 11. Validation of RAB11B-AS1 expression in 3 cell lines.

4. Discussion

EC is among the three major malignant tumors affecting the female reproductive system. Its incidence is progressively increasing, particularly in younger individuals [21]. Currently, commonly employed screening methods for EC, such as tumor markers and vaginal ultrasound, have limitations in terms of sensitivity, specificity, and effectiveness. While endometrial biopsy serves as the gold standard for EC diagnosis, its invasiveness restricts routine recommendation [22]. Therefore, there is an urgent need to identify effective biomarkers for EC. Disulfidptosis, a novel form of cell death, has emerged as a potential application in tumor therapy. Several studies have demonstrated that disulfidptosis can contribute to the antitumor effects of certain chemotherapeutic drugs, including cisplatin and paclitaxel, through intracellular disulfide reactions [23, 24]. The significance of long noncoding RNAs (lncRNAs) in EC is increasingly recognized. LncRNA transcripts, consisting of over 200 nucleotides, are involved in various biological processes, including tumor cell apoptosis, cell cycle regulation, migration, differentiation, and proliferation [25]. Importantly, aberrant expression of certain lncRNAs has been observed in EC tissues compared to normal endometrial tissues. For instance, Dong *et al.* identified DLEU2 as an upstream activator of HK2-driven epithelial-mesenchymal transition (EMT) and glycolysis in EC cells, providing significant mechanistic insights for potential EC treatment [26]. Jiang *et al.* discovered that knockdown of carcinogenic LINC00958 inhibited the growth and metastasis of EC cells [27]. However, to date, no studies have investigated the role of DRLs in EC. Therefore, this study aims to establish a risk signature based on DRLs in EC.

In this study, we conducted screening using univariate Cox regression analysis, LASSO regression analysis, and multivariate Cox regression analysis, which revealed that Z69733.1, AL158071.4, AC005034.2, AC003086.1, and AL499602.1 may serve as poor prognostic factors in patients with EC, while AC022960.1, AC024230.1, and RAB11B-AS1 may act as protective factors. The RAB protein family consists of highly conserved small GTP proteins that regulate activity in various cells. Over 70 types of RAB proteins have been identified and are widely distributed in the cell membrane structures of multiple cells, with RAB11B-AS1 being one of them [28, 29]. Studies have demonstrated that dysregulation of different members of the RAB11 subfamily can impact tumor invasion and metastasis in various tumors, including lung cancer, gastric cancer, and renal cell carcinoma [4-6]. Recent research has also explored the role of RAB11B-AS1 in tumors. For example, Dai *et al.* found downregulation of RAB11B-AS1 in hepatocellular carcinoma, correlating with poor prognosis [20]. Bovine *et al.* identified upregulation of RAB11B-AS1 in breast cancer, enhancing the expression of angiogenic factors in hypoxic breast cancer cells [30]. Therefore, the significance of RAB11B-AS1 in tumors supports the reliability of our study results. Thus, there are additional reasons to further investigate and study other DRLs. Subsequently, we constructed a prognostic signature. The KM survival curve, ROC curve, and nomogram validated the overall accuracy of the model for predicting the prognosis of EC patients, confirming that the model composed of 8 DRLs was an independent prognostic factor for EC. Furthermore, PCA demonstrated that our model outperformed other models in distinguishing between high-risk and low-risk EC patients. Additionally, we performed functional enrichment analysis, which revealed that these DRLs were enriched in functions such as "receptor ligand activity," "immunoglobulin complex," "circulating," and "IgA immunoglobulin complex". This finding supported the plausible association between disulfidptosis and

immunotherapy.

We proceeded to investigate the association among TMB, immune-related function, and risk scores in patients with EC. Previous studies have consistently demonstrated that TMB serves as an independent prognostic factor capable of predicting immunotherapy efficacy in various tumor types [31-33]. In our analysis, we computed the TMB for both the high- and low-risk groups and observed a higher frequency of TP53 mutations in the high-risk group than in the low-risk group. Notably, a few studies have reported that TP53 mutations can enhance antitumor immune activity and responsiveness to immunotherapy [34, 35]. This observation may account for the better survival outcomes in the high TMB group than in the low TMB group. Additionally, we found that the high TMB group exhibited significantly improved prognosis. Considering the vital role of the TME in immunology, encompassing immune checkpoint inhibitor (ICI) expression levels, tumor immune infiltrating cell (TIIC) infiltration, and cancer immune circuitry [27], we detected substantial disparities in immune cell infiltration, immune function, and TIDE between the two risk groups based on the DRL-derived signature. These findings might serve as a guide for immunotherapy strategies in EC patients and contribute to understanding the potential link between tumor immunity and disulfidptosis in colorectal cancer. Finally, we conducted an analysis to assess the sensitivity of different risk groups to various chemotherapy drugs and identified nine therapeutic agents exhibiting significant differences, suggesting their potential as treatment options for EC. Finally, we examined the expression of RAB11B-AS1 in normal endometrial cells and EC cell lines using qRT-PCR, and in agreement with the results of the bioinformatics analysis, its expression was down-regulated in EC cells.

Our study possesses several limitations. First, there is a scarcity of research on DRLs in EC, and the underlying molecular mechanisms of DRLs in EC remain to be elucidated. Second, the lack of an appropriate EC project in the GEO database prevents us from conducting external validation. Besides, although we determined that RAB11B-AS1 is lowly expressed in EC cells, further experiments are still needed to investigate whether it affects the proliferation, invasion and migration ability of EC cells and the possible molecular mechanisms.

5. Conclusion

We employed bioinformatics methods to screen 8 DRLs and developed a prognostic risk model for predicting the outcomes of EC patients. Furthermore, we investigated the associations between risk score-based groups and TMB, TME, TIDE, and drug sensitivity. In summary, our study not only sheds light on the role of DRLs in EC but also offers novel insights into predicting patient survival and clinical treatment efficacy in EC.

Acknowledgements

The authors thank the staff members of TCGA, PubMed, TIDE.

Author contributions

YZ and HL designed the research. YZ completed all analysis in the research. YZ and HL drafted the manuscript. QL participated in the critical revision of the manuscript and provided support in English polishing work. YW, XL, QJ, HZ, and HZ participated in the manuscript's data collection and literal modification. HL supervised the whole study process. All authors read and approved the final manuscript.

Funding

This study was supported in part by grants from the National Natural Science Foundation of China (82272332) and by grants from the Joint Project of Henan Medical Science and Technology Research Plan (SBGJ202002091).

Availability of data and materials

The datasets used and/or analysed during the current study available from the corresponding author on reasonable request.

Declarations

Ethics approval and consent to participate

TCGA belongs to public databases. The patients involved in the databases have obtained ethical approval. Users

can download relevant data for free for research and publish relevant articles. Our study is based on open source data, so there are no ethical issues and other conflicts of interest.

Consent for publication

Not applicable.

Competing interests

The authors declare that they have no known competing financial interests or personal relationships that could have appeared to influence the work reported in this paper.

References

- [1] Bray F, Ferlay J, Soerjomataram I, Siegel RL, Torre LA, Jemal. GLOBOCAN estimates of incidence and mortality worldwide for 36 cancers in 185 countries. *Ca Cancer J Clin.*, 2018, 68(6):394-424.
- [2] Makker V, MacKay H, Ray-Coquard I, Levine DA, Westin SN, Aoki D, Oaknin A. Endometrial cancer. *Nature Reviews Disease Primers*, 2021, 7(1):88.
- [3] Brooks RA, Fleming GF, Lastra RR, Lee NK, Moroney JW, Son CH, Tatebe K, Veneris JL. Current recommendations and recent progress in endometrial cancer. *CA: A Cancer Journal for Clinicians*, 2019, 69(4):258-279.
- [4] Tang D, Kang R, Berghe TV, Vandenabeele P, Kroemer G. The molecular machinery of regulated cell death. *Cell Research*, 2019, 29(5):347-364.
- [5] Edoui S, Herold MJ, Strasser A. Emerging connectivity of programmed cell death pathways and its physiological implications. *Nature Reviews Molecular Cell Biology*, 2020, 21(11):678-695.
- [6] Tsvetkov P, Coy S, Petrova B, Dreishpoon M, Verma A, Abdusamad M, Rossen J, Joesch-Cohen L, Humeidi R, Spangler RD. Copper induces cell death by targeting lipoylated TCA cycle proteins. *Science*, 2022, 375(6586):1254-1261.
- [7] Liu X, Nie L, Zhang Y, Yan Y, Wang C, Colic M, Olszewski K, Horbath A, Chen X, Lei G. Actin cytoskeleton vulnerability to disulfide stress mediates disulfidptosis. *Nature Cell Biology*, 2023, 25(3):404-414.
- [8] Liu X, Olszewski K, Zhang Y, Lim EW, Shi J, Zhang X, Zhang J, Lee H, Koppula P, Lei G. Cystine transporter regulation of pentose phosphate pathway dependency and disulfide stress exposes a targetable metabolic vulnerability in cancer. *Nature Cell Biology*, 2020, 22(4):476-486.
- [9] Zheng P, Zhou C, Ding Y, Duan S. Disulfidptosis: a new target for metabolic cancer therapy. *Journal of Experimental & Clinical Cancer Research*, 2023, 42(1):103.
- [10] Zhong Z, Zhang C, Ni S, Ma M, Zhang X, Sang W, Lv T, Qian Z, Yi C, Yu B. NFATc1-mediated expression of SLC7A11 drives sensitivity to TXNRD1 inhibitors in osteoclast precursors. *Redox Biology*, 2023, 63:102711.
- [11] Atianand MK, Caffrey DR, Fitzgerald KA. Immunobiology of long noncoding RNAs. *Annual Review of Immunology*, 2017, 35:177-198.
- [12] Cech TR, Steitz JA. The noncoding RNA revolution—Trashing Old Rules to Forge New Ones. *Cell*, 2014, 157(1):77-94.
- [13] Guttman M, Russell P, Ingolia NT, Weissman JS, Lander ES. Ribosome profiling provides evidence that large noncoding RNAs do not encode proteins. *Cell*, 2013, 154(1):240-251.
- [14] Moran VA, Perera RJ, Khalil AM. Emerging functional and mechanistic paradigms of mammalian long non-coding RNAs. *Nucleic Acids Research*, 2012, 40(14):6391-6400.
- [15] Bhan A, Soleimani M, Mandal SS. Long noncoding RNA and cancer: a new paradigm. *Cancer Research*, 2017, 77(15):3965-3981.
- [16] Fang Y, Fullwood MJ. Roles, functions, and mechanisms of long non-coding RNAs in cancer. *Genomics, Proteomics & Bioinformatics*, 2016, 14(1):42-54.
- [17] Chi Y, Wang D, Wang J, Yu W, Yang J. Long non-coding RNA in the pathogenesis of cancers. *Cells*, 2019, 8(9):1015.
- [18] Renhua G, Yue S, Shidai J, Jing F, Xiyi L. 165P: Long noncoding RNA LUCAT1 is associated with poor prognosis in human non-small cell lung cancer and affects cell proliferation via regulating p21 and p57 expression. *Journal of Thoracic Oncology* 2016, 11(4):S129.
- [19] Cao H, Liu Z, Huang P, Yue Y, Xi J. lncRNA-RMRP promotes proliferation, migration and invasion of bladder cancer via miR-206. *Eur Rev Med Pharmacol Sci.*, 2019, 23(3):1012-1021.
- [20] Dai Y-z, Liu Y-d, Li J, Chen M-t, Huang M, Wang F, Yang Q-s, Yuan J-h, Sun S-h. METTL16 promotes hepatocellular

- carcinoma progression through downregulating RAB11B-AS1 in an m6A-dependent manner. *Cellular & Molecular Biology Letters*, 2022, 27(1):41.
- [21] Lee YC, Lheureux S, Oza AM. Treatment strategies for endometrial cancer: current practice and perspective. *Current Opinion in Obstetrics and Gynecology*, 2017, 29(1):47-58.
- [22] Braun MM, Overbeek-Wager E, Grumbo RJ. Diagnosis and management of endometrial cancer. *American Family Physician*, 2016, 93(6):468-474.
- [23] Sideris S, Aoun F, Zanaty M, Martinez NC, Latifyan S, Awada A, Gil T. Efficacy of weekly paclitaxel treatment as a single agent chemotherapy following first-line cisplatin treatment in urothelial bladder cancer. *Molecular and Clinical Oncology*, 2016, 4(6):1063-1067.
- [24] Mitin T, Hunt D, Shipley WU, Kaufman DS, Uzzo R, Wu C-L, Buyyounouski MK, Sandler H, Zietman AL. Transurethral surgery and twice-daily radiation plus paclitaxel-cisplatin or fluorouracil-cisplatin with selective bladder preservation and adjuvant chemotherapy for patients with muscle invasive bladder cancer (RTOG 0233): a randomised multicentre phase 2 trial. *The Lancet Oncology*, 2013, 14(9):863-872.
- [25] Abdi E, Latifi-Navid S, Latifi-Navid H. LncRNA polymorphisms and breast cancer risk. *Pathology-Research and Practice*, 2022, 229:153729.
- [26] Dong P, Xiong Y, Konno Y, Ihira K, Kobayashi N, Yue J, Watari H. Long non-coding RNA DLEU2 drives EMT and glycolysis in endometrial cancer through HK2 by competitively binding with miR-455 and by modulating the EZH2/miR-181a pathway. *Journal of Experimental & Clinical Cancer Research*, 2021, 40(1):1-16.
- [27] Jiang Y, Qiao Z, Jiang J, Zhang J. LINC00958 promotes endometrial cancer cell proliferation and metastasis by regulating the miR-145-3p/TCF4 axis. *The Journal of Gene Medicine*, 2021, 23(7):e3345.
- [28] Homma Y, Hiragi S, Fukuda M. Rab family of small GTPases: an updated view on their regulation and functions. *The FEBS Journal*, 2021, 288(1):36-55.
- [29] Pfeffer SR. Rab GTPases: master regulators that establish the secretory and endocytic pathways. *Molecular Biology of the Cell* 2017, 28(6):712-715.
- [30] Niu Y, Bao L, Chen Y, Wang C, Luo M, Zhang B, Zhou M, Wang JE, Fang YV, Kumar A. HIF2-Induced Long Noncoding RNA RAB11B-AS1 Promotes Hypoxia-Mediated Angiogenesis and Breast Cancer Metastasis RAB11B-AS1 Promotes Angiogenesis and Breast Tumor Metastasis. *Cancer Research*, 2020, 80(5):964-975.
- [31] Sha D, Jin Z, Budczies J, Kluck K, Stenzinger A, Sinicrope FA. Tumor mutational burden as a predictive biomarker in solid tumors. *Cancer Discovery*, 2020, 10(12):1808-1825.
- [32] Yarchoan M, Hopkins A, Jaffee EM. Tumor mutational burden and response rate to PD-1 inhibition. *New England Journal of Medicine*, 2017, 377(25):2500-2501.
- [33] Samstein RM, Lee C-H, Shoushtari AN, Hellmann MD, Shen R, Janjigian YY, Barron DA, Zehir A, Jordan EJ, Omuro A. Tumor mutational load predicts survival after immunotherapy across multiple cancer types. *Nature Genetics*, 2019, 51(2):202-206.
- [34] Textor S, Fiegler N, Arnold A, Porgador A, Hofmann TG, Cerwenka A. Human NK Cells Are Alerted to Induction of p53 in Cancer Cells by Upregulation of the NKG2D Ligands ULBP1 and ULBP2 ULBP1 and ULBP2 Are Direct p53 Target Genes. *Cancer Research*, 2011, 71(18):5998-6009.
- [35] Dong Z-Y, Zhong W-Z, Zhang X-C, Su J, Xie Z, Liu S-Y, Tu H-Y, Chen H-J, Sun Y-L, Zhou Q. Potential predictive value of TP53 and KRAS mutation status for response to PD-1 blockade immunotherapy in lung adenocarcinoma. *Clinical Cancer Research*, 2017, 23(12):3012-3024.